Attoclock Photoelectron Interferometry with Two-Color Corotating Circular Fields to Probe the Phase and the Amplitude of Emitting Wave Packets

Meng Han, Peipei Ge, Yun Shao, Qihuang Gong, and Yunquan Liu

Phys. Rev. Lett. **120**, 073202 — Published 15 February 2018

DOI: 10.1103/PhysRevLett.120.073202

Attoclock photoelectron interferometry with two-color corotating circular fields to probe the phase and the amplitude of emitting wave packets

Meng Han[1], Peipei Ge[1], Yun Shao[1], Qihuang Gong[1,3], Yunquan Liu[1,2,3,4*]

[1]*School of Physics and State Key Laboratory for Mesoscopic Physics, Peking University, Beijing 100871, China*

[2]*Center for Applied Physics and Technology, HEDPS, Peking University, Beijing 100871, China*

[3]*Collaborative Innovation Center of Quantum Matter, Beijing 100871, China*

[4]*Collaborative Innovation Center of Extreme Optics, Shanxi University, Taiyuan, Shanxi 030006, China*

Abstract: We employ attosecond angular streaking with photoelectron interferometric metrology to reveal electron sub-Coulomb-barrier dynamics. We use a weak perturbative co-rotating circularly polarized field (800 nm) to probe the strong-field ionization by an intense circularly polarized field (400 nm). In this double-hand attoclock photoelectron interferometry, we introduce a spatially rotating temporal Young's two-slit interferometer, in which the oppositely modulated wave-packets originating from consecutive laser cycles are dynamically prepared and interfered. Developing a Fourier-transform algorithm on energy-resolved photoelectron interferograms, we can directly extract the amplitude and the phase of emitting electron wave packets from strong-field ionization.

PACS numbers: 33.80.Rv 31.90.+s

Coherent imaging of electron wave-packets has attracted wide interest in modern sciences [1]. For strong-field ionization, the amplitude and the phase of the ionized electron wave-packet could give direct insights of electron dynamics in the classically-forbidden, sub-Coulomb-barrier region. Benefiting from that the laser pulse duration approaches to the natural timescale of intra-atomic electron dynamics, one was allowed to image the amplitude or the phase of an electron wavefunction on the attosecond scale, such as measuring the angular components of the wave-packet with attosecond pulse trains synchronized with an infrared light field [2], probing bound-state wave-packets in a pump-probe scheme [3], and extracting the Coulomb scattering phase from photoelectron holography [4].

Alternatively, using a circularly-polarized femtosecond laser pulse, dubbed as attosecond angular streaking or attoclock [5-9] (the rotating laser electric vector looks like a clock hand), one can transform the rotation of the clock-hand polarization to the attosecond time resolution. Using the circular polarization, the rescattering of the liberated electron with its parent ion can be avoided and the electron is considered to move classically. Thus, the electron momentum will be approximately shown to point at an angle of 90^{o} relative to the laser electric-field direction at the ionizing instant. In attoclock experiments [5-9], the photoelectron interference effect has been ignored. Indeed, interference structure in photoelectron momentum distribution contains fruitful information. Generally, at a given time t_0 in circular polarization, an ionized electron wave-packet (EWP) can be described as $\psi_0 = W_0 e^{i\varphi_0}$, where W_0 is the amplitude and φ_0 is the phase. This wave-packet will interfere with the subsequent EWP that is emitted after one laser period T at a radial direction of the momentum plane (inter-cycle interference). The interferogram of the two EWPs is given by $I^{(\mathrm{one})} = |\psi_0 + \psi_0 e^{ib}|^2$ [$b = -\int_{t_0}^{t_0+T} [\boldsymbol{p} + \boldsymbol{A}(t)]^2/2 + I_p dt = -(\boldsymbol{p}^2/2 + U_p + I_p)T$ is the phase difference due to their temporal separation, where $\boldsymbol{p}$ is the canonical momentum, $\boldsymbol{A}(t)$ is the laser vector potential, I_p is the ionization potential, and U_p is the ponderomotive energy]. It appears as above-threshold ionization (ATI) peaks with one photon energy interval [10].

Recently, the two-color counter-rotating circular fields have been used to produce high harmonics of circular polarization [11,12], to control above threshold ionization [13] and to enhance double ionization [14,15]. In those cases, substantial rescattering events will take place. For the two-color co-rotating circular fields with comparable

intensities, the ionization from both fields has the significant contribution to the photoelectron momentum distributions [13], so that it is hard to establish the attoclock to probe the sub-barrier dynamics.

In this Letter, employing two-color co-rotating circular fields, we demonstrate a double-hand attoclock photoelectron interferometer to probe the phase and the amplitude of emitting wave packets from strong-field ionization. To that end, we manipulate the rotating barrier on both radial and angular directions, by adding a perturbative co-rotating laser field at the half frequency of the ionizing laser pulse [see Fig. 1(a)]. The synthesized laser field is $\boldsymbol{E}(t)=[E_{400}\cos(\omega t)+E_{800}\cos(0.5\omega t+\varphi_L)]\boldsymbol{z}$ $+[E_{400}\sin(\omega t)+E_{800}\sin(0.5\omega t+\varphi_L)]\boldsymbol{x}$, where φ_L is the phase delay between the two pulses. The intense second harmonic field (400 nm) is used to ionize atoms [16]. The fundamental wave (800 nm) is a very weak perturbative probe pulse, and its intensity is controlled to be below 0.5% of the ionizing field.

This is equal to adding an hour hand (800 nm) into an attoclock that possesses only a single minute hand (400 nm). The hour hand will break the symmetry of the original light field, so that both the amplitude and the phase of emitting EWPs are modified accordingly. One can describe the modulated EWP as $\psi_0 e^{-i\varepsilon}$ with a small complex quantity ε, where its real part (Re[ε]) is the phase variation as $\varphi=\varphi_0$-Re[ε] and its imaginary part (Im[ε]) corresponds to the amplitude modification as $W=W_0 e^{\mathrm{Im}[\varepsilon]}$. The imaginary phase Im[ε] is related with the ionization probability, which originates from the sub-barrier process since the classical propagation outside the barrier approximately does not change its probability amplitude [17]. At ionization instants of the interfered EWPs, i.e., t_0 and $t_0 + T_{400}$, the electron feels the opposite force of the hour hand under the barrier. The two laser-induced EWPs appear opposite modifications as $\psi_0 e^{-i\varepsilon}$ and $\psi_0 e^{i\varepsilon}$ [see Fig. 1(b)], imprinting the subtle sub-barrier effects on its amplitude and phase distributions. For different ionization times, the bent potential barrier rotates and the emitting EWPs will be streaked to different radial directions. Therefore, this scheme can be viewed as a spatially-rotating temporal Young's two-slit interferometer.

To reveal the effect of the modulation, in Fig. 1(c), we show the photoelectron momentum distributions in one-color and in two-color circular fields at $\varphi_L = 0$, calculated by the strong-field approximation (SFA) model [18]. In the SFA model, after ionization the Coulomb potential is ignored and the mapping relationship between the electron ionization time t_0 and emitting angle θ is strictly established. The

transition matrix element is given by $M_{\boldsymbol{p}}^{(\mathrm{SFA})} \sim \int_0^{t_f} d\tau \frac{[\boldsymbol{p}+\boldsymbol{A}(\tau)]\cdot \boldsymbol{E}(\tau)}{\pi\{[\boldsymbol{p}+\boldsymbol{A}(\tau)]^2+2I_p\}^3} \exp\{\int_0^{\tau} \frac{1}{2}[\boldsymbol{p}+\boldsymbol{A}(t')]^2 + I_p dt'\}$, where t_f is the pulse turn-off time, and I_p is selected as 0.579 a.u. to match argon atoms. The laser field is synthesized by a six-cycle $\sin^2$-envelope laser pulse at 800 nm, and the peaks of 800 nm and 400 nm electric fields are $E_{400} = 0.04$ a.u. and $E_{800} = 0.0025$ a.u., respectively.

Within the SFA, an EWP will be streaked to the angle θ perpendicular to the direction of the ionizing field $E_{400}(t_0)$, which is the ionizing (or "minute") hand. Thus, the location of the interference fringes among the paired EWPs in Fig. 1(b) can be uniquely determined, which is marked by the blue arrow in Fig. 1(c). In time domain, a weak probe light will break the homogeny of these EWPs and their interference leads sidebands (SBs) to emerge between the adjacent ATIs, having the angle-dependent feature.

The SBs are involved with the inter-cycle photoelectron interference of 800 nm field. Thus, the photoelectron momentum distribution in this two-color fields [Fig. 1(c), right], can be generally described by the four-EWP interference within two periods of 800 nm field as $I^{(\mathrm{two})}=|\psi_0 e^{-i\varepsilon}+\psi_0 e^{i\varepsilon+ib}+\psi_0 e^{-i\varepsilon+i2b}+\psi_0 e^{i\varepsilon+i3b}|^2$. The angle- and energy- resolved photoelectron interferogram can be expressed as,

$$\begin{aligned} I^{(\mathrm{two})}(\theta, E_\theta) = {} & 2W_0^2(e^{-2\mathrm{Im}[\varepsilon]}+e^{2\mathrm{Im}[\varepsilon]}) + 4W_0^2\cos(E_\theta T_{400} + 2\,\mathrm{Re}[\varepsilon] + a) \\ & + 2W_0^2\cos(E_\theta T_{400} - 2\,\mathrm{Re}[\varepsilon] + a) + 2W_0^2(e^{-2\mathrm{Im}[\varepsilon]}+e^{2\mathrm{Im}[\varepsilon]})\cos(2E_\theta T_{400} + 2a) \\ & + 2W_0^2\cos(3E_\theta T_{400} + 2\,\mathrm{Re}[\varepsilon] + 3a). \end{aligned} \tag{1}$$

Here $a=(U_p+I_p)T_{400}$ is a constant phase. In frequency domain, the SB emission corresponds to the absorption or emission of a single 800 nm photon from adjacent ATIs, as clearly shown in the electron energy spectrum at an emission angle of 90° [Fig. 1(d)]. In the supplementary material (SM), we have substituted the experimental measured phase into Eq. (1) and have tested the four wave-packet interference geometry by retrieving the photoelectron momentum distribution.

Experimentally, the two-color circularly polarized fields were generated using a Mach-Zehnder interferometer scheme. The fundamental laser pulse (wavelength ~ 800 nm, pulse duration ~ 25 fs) was derived from a Ti:sapphire multipass amplifier operating at 3 kHz. The second harmonic was obtained via frequency doubling in a 250-μm-thick β-Barium Borate (BBO) crystal. The relative time delay of the two pulses was controlled by a pair of wedges. The electron momentum distributions of argon

atoms were measured by cold-target recoil-ion reaction momentum spectroscopy (COLTRIMS) [19]. The intensity of the 400 nm light was calibrated to be ~ $(1.1\pm0.2)\times10^{14}$ W/cm^2 by ATI locations, and that of the 800 nm light was calibrated ~ $(0.44\pm0.05)\times10^{12}$ W/cm^2 by comparing electron momentum distributions with the *ab initio* simulations. In the experiment, one needs to realize the perfect circular polarizations for both fields. The experimental setup is presented in SM in detail.

Figs. 2(a) and 2(b) show the measured photoelectron momentum distributions in one-color circular field and in two-color circular fields at $\varphi_L = 0$, respectively. After adding the perturbative 800 nm field, both ATIs and SBs show the angle-dependent feature. Noted that those two spectra are measured at the same laser pulse at 400 nm. As shown in Fig. 2(b), along the negative p_x axis, the ATI yields are much higher than the SB yields, and the situation is reversed along the positive direction. The calculations by the SFA model agree with the experiments. By comparison with the results in Fig. 1(c), one can see that the angle dependences and variation ranges of ATI and SB peaks are well coincident. We also calculate the photoelectron momentum distributions by the *ab initio* method with numerically solving time-dependent Schrödinger equation (TDSE) [20]. The calculation by the SFA shows the similar distribution with the result by the TDSE method (see SM), suggesting that the SFA is a good approximation for current experimental condition.

To extract the complex phase of wave packets, we transform the electron momentum distribution into angle-resolved energy distribution $I(\theta, E_\theta)$. With this, the equally-spaced ATI and SB peaks behaves like equally-spaced interference fringes [see SM for experimental data or Fig. 1(d)], in analogy with traditional optical interferometry [21]. One can see that in this photoelectron interferogram, the amplitude and the phase carried by the EWPs are recorded by the interferometer into a clear modulation of ATI and SB peaks. In traditional optical interferometry, the real-space optical interferogram, $I(x,y)$, can always be described by $I(x, y)=I_0(x, y)+a(x, y)\cos[2\pi f_x x+\varphi(x, y)]$, where f_x is the fringe frequency in the x direction, $\varphi(x, y)$ is the pattern phase contained in the interference term, $I_0(x, y)$ is the interferogram background (also called zero-frequency component), and $a(x, y)$ describes variations of the fringe visibility. All the components of the interferogram can be extracted through a Fourier-transform approach [21].

In this double-hand attoclock photoelectron interferometry, the electron streaked angle θ and the energy E_θ along the polar angle are in analogy with the y and x, respectively. As seen from Eq. (1), $2W_0^2e^{2\mathrm{Im}[\varepsilon]}+2W_0^2e^{-2\mathrm{Im}[\varepsilon]}$ (the probability superposition of the two modulated wave-packets) corresponds to the background $I_0(x, y)$. The real part of the complex phase corresponds to the pattern phase, i.e., $\varphi(x, y) \sim 2\mathrm{Re}[\varepsilon]$. For the one-color interferogram, $I_0(x, y)$ corresponds to $4W_0^2$ (the probability of two identical unmodulated wave-packets) and $\varphi(x, y)$ is a constant number.

The 2D complex phase can be fully extracted using a Fourier-transform algorithm from the electron momentum distributions [Figs. 2(a) and 2(b)]. First, we transform the momentum distributions to angle-resolved energy spectra and do the Fourier transform along each θ. To extract $\mathrm{Im}[\varepsilon]$, we filter out the interference terms from the obtained Fourier spectra, recover the zero-frequency component by the inverse transform, and then utilize the ratio [corresponding to $1/2(e^{2\mathrm{Im}[\varepsilon]}+ e^{-2\mathrm{Im}[\varepsilon]})$] between the two-color and one-color results to evaluate $\mathrm{Im}[\varepsilon]$. To extract $\mathrm{Re}[\varepsilon]$, in the two-color Fourier spectrum we shift the frequency component of the interference term [corresponding to $2W_0^2\cos(3E_\theta T_{400}+2\mathrm{Re}[\varepsilon]+3a)$] to the center, and do the inverse transform along each θ. Then we can obtain $2\mathrm{Re}[\varepsilon]$ (it is proportional to the argument of the obtained complex number). The algorithm and the extraction process are presented in SM. Note that the phase reconstruction method is a pure mathematic approach, which is independent with any tunneling or multi-photon models of strong-field ionization. In the deep tunneling regime, photoelectron holography [22] has been demonstrated. However, it is hard to read the information from the hologram. Here, concentrating on the time-resolved interference patterns, we can extract the amplitude and the phase of wave packets.

Figures 2(c) and 2(d) show the extracted real phase $\mathrm{Re}[\varepsilon]$ and imaginary phase $\mathrm{Im}[\varepsilon]$ with respect to the emission angle. We illustrate the corresponding ionization instants using a clock on the top of the panels (the angle bin size is 2° and the time resolution ~ 8 as). From the distributions, one can see that the modulation at the most probable momentum is less for both the real and the imaginary phase, and the two flanks of the EWP are affected mostly when the probing perturbative field is on. When the two hands of the attoclock are parallel (θ = 180°), the Coulomb barrier is bent further by the short clock hand to the same direction, and the emitting EWP will become wider and its center location is not changed obviously. Thus, along the

direction the real phase has the minima at the central part, and the imaginary phase shows that the high-momentum part of the EWP is most enhanced, indicating the sub-barrier process serves as a high-pass filter in momentum space. When the two clock hands are perpendicular ($\theta = 0°$), the EWP experiences a lateral force under the barrier, and the force will change its peak location and rearrange the phase remarkably. Thus, along the direction the real phase oscillates obviously, and the imaginary phase indicates that the lateral shift of the EWP causes its two flanks slight enhancement.

From the extracted imaginary phase, we are able to image the momentum distribution of EWP when it emerges from atoms. To that end, one needs to subtract the laser-streaking momentum ($E_{400}/\omega \approx 0.351$ a.u.) from the measured momentum. First, we reconstruct the background $4W_0(\theta, P_\theta)^2$ from the one-color interferogram through inversely transforming its zero-frequency component in the Fourier spectrum, then reduce the streaking momentum. Using the relation of the streaking angle θ to the birth time t_0, the momentum distribution of EWP $W_0(t_0, P_{\text{exit}})$ in single circular field (400 nm) at the birth time is obtained, as shown in Fig. 3(a). It is shown that the transversal momentum of EWP is not centered at zero when the EWP is freed, because the electron experiences the rotating force under the barrier, reflecting the non-adiabatic nature of the interaction between laser fields and atoms [23,24]. Combining the extracted time-resolved Im[ε] [Fig. 2(d)] with the extracted $W_0(t_0, P_{\text{exit}})$, in Fig. 3(b) we reconstruct the evolution of the modulated EWP using $W(t_0, P_{\text{exit}}) = W_0(t_0, P_{\text{exit}})e^{\text{Im}[\varepsilon]}$. From $t_0 = 0$ to $t_0 = T_{400}/2$, the two clock hands are rotating from parallel to vertical and the probability of EWP decreases nonlinearly. The ionized flux is highly dependent on the electric-field component along the long clock-hand direction. The emitting wave-packet is dynamically imaged within the resolution of a few attoseconds. The theoretical work [23,25] have pointed the initial momentum will shift in a circular field and recent experiments [9,26] verified the prediction.

It is worth mentioning that there is another working mode of the double-hand attoclock photoelectron interferometer. If one focuses on a certain radial direction of photoelectron momentum distribution (P_θ) at a given θ, and then scans the laser phase delay φ_L to measure the interferogram variation along the direction, it is equal to fixing the long clock-hand direction and rotating the short clock hand, rather than the two-hand simultaneously rotating in Fig. 2. Figures 4(a) and 4(b) depict the measured

momentum distribution at two radial directions (along positive p_z and along negative p_z) with respect to the phase delay in one cycle of 800 nm field. The ATI and SB peaks oscillate alternately with the time delay of roughly $T_{400}/2$ and the polarizations of the two clock hands are shown at the top of the figures. We retrieved the background term $2W_0^2e^{2\mathrm{Im}[\varepsilon]}+ 2W_0^2e^{-2\mathrm{Im}[\varepsilon]}$ for above two distributions through the extraction algorithm. The difference between the backgrounds is shown in Fig. 4(c). In the result, it is clear that the ATI peaks are dominant when the two clock hands are parallel and the SBs are dominant when they are perpendicular.

In Fig. 4(d), we give an interpretation on the formation of ATIs and SBs. For the two-hand parallel case, the potential barrier is lifted or lowered by the weak clock hand, and the emitting EWPs are not segregated in the momentum space, so the ATI peaks are dominant. Whereas for the orthogonal case, the lateral force will shift the EWPs into reverse directions, so that the EWPs are not well overlapped and the ATIs will be weak. The phase variation of the EWP causes the interference fringes to shift significantly, and thus the SB peaks are dominant.

In conclusion, we introduce a novel double-hand attoclock photoelectron interferometer to probe the electron sub-barrier dynamics. This photoelectron interferometry largely extends the capacity of attosecond angular streaking, equipped with the ability of photoelectron interferometric metrology. The measured photoelectron angular distributions are in perfect circular polarization, allowing us to extract the phase and the amplitude of the emitting wave packets. The initial momentum distribution of emitting electron wavepackets can be well characterized by this approach. This study provides direct insights into the basic properties of laser-induced ionization, following the evolution of the atomic electronic wave-function within the temporal resolution of several attoseconds. The double-hand attoclock photoelectron interferometer could be used to further explore the oriented molecules to image molecular electronic wave-functions.

This work is supported by the National Science Foundation of China (Grant No. 11434002, 11774013 and 11527901).

*Yunquan.liu@pku.edu.cn

References

[1] M. J. J. Vrakking, *Phys. Chem. Chem. Phys.* **16**, 2775 (2014).

[2] D. M. Villeneuve, P. Hockett, M. J. J. Vrakking, and H. Niikura, *Science* **356**, 1150–1153 (2017).

[3] J. Mauritsson *et al.*, *Phys. Rev. Lett.* **105**, 053001 (2010).

[4] Y. Zhou, O. I. Tolstikhin, and T. Morishita, *Phys. Rev. Lett.* **116**, 173001 (2016).

[5] P. Eckle, A. N. Pfeiffer, C. Cirelli, A. Staudte, R. Dörner, H. G. Muller, M. Büttiker, and U. Keller, *Science* **322**, 1525 (2008).

[6] P. Eckle, M. Smolarski, P. Schlup, J. Biegert, A. Staudte, M. Schöffler, H. G. Muller, R. Dörner, and U. Keller, *Nat. Phys*. **4**, 565 (2008).

[7] L. Torlina *et al.*, Nat. Phys. **11**, 503 (2015).

[8] M. Li, Y. Liu, H. Liu, Q. Ning, L. Fu, J. Liu, Y. Deng, C. Wu, L. Y. Peng, and Q. Gong, *Phys. Rev. Lett.* **111**, 023006 (2013).

[9] M. Li, M.-M. Liu, J.-W. Geng, M. Han, X. Sun, Y. Shao, Y. Deng, C. Wu, L.-Y. Peng, Q. Gong, and Y. Liu, *Phys. Rev. A* **95**, 053425 (2017).

[10] P. Agostini, F. Fabre, G. Mainfray, G. Petite, and N. K. Rahman, *Phys. Rev. Lett.* **42**, 1127 (1979).

[11] O. Kfir *et al.*, *Nat. Photon.* **9**, 99 (2014).

[12] A. Fleischer, O. Kfir, T. Diskin, P. Sidorenko, and O. Cohen, *Nat. Photon.* **8**, 543 (2014).

[13] C. A. Mancuso *et al.*, *Phys. Rev. A* **91**, 031402 (2015).

[14] S. Eckart *et al.*, *Phys. Rev. Lett.* **117,** 133202 (2016).

[15] C. A. Mancuso *et al.*, *Phys. Rev. Lett.* **117**, 133201 (2016).

[16] X. Xie *et al.*, *Phys. Rev. Lett.* **119**, 243201 (2017).

[17] O. Pedatzur *et al.*, *Nature Physics* **11**, 815 (2015).

[18] D. B. Milošević, G. G. Paulus, D. Bauer, and W. Becker, *J. Phys. B* **39**, R203 (2006).

[19] J. Ullrich, R. Moshammer, A. Dorn, R. Dörner, L. Ph. H. Schmidt, and H. Schmidtböcking, *Rep. Prog. Phys.* **66**, 1463 (2003).

[20] V. Mosert and D. Bauer, *Comput. Phys. Commun.* **207**, 452 (2016).

[21] M. Takeda, H. Ina, and S. Kobayashi, *J. Opt. Soc. Am*. **72**, 156 (1982).

[22] Y. Huismans *et al.*, *Science* **331**, 61 (2011).

[23] M. Han, M. Li, M.-M Liu, and Y. Liu, *Phys. Rev. A* **95**, 023406 (2017).

[24] M. Han, P. Ge, Y. Shao, M.-M Liu, Y. Deng, C. Wu, Q. Gong, and Y. Liu, *Phys. Rev. Lett.* **119**, 073201 (2017).

[25] I. Barth and O. Smirnova, *Phys. Rev. A* **84**, 063415 (2011).

[26] M.-M Liu, M. Li, Y. Shao, M. Han, Qihuang Gong, and Yunquan Liu, *Phys. Rev. A* **96**, 043410 (2017).

Figure legends

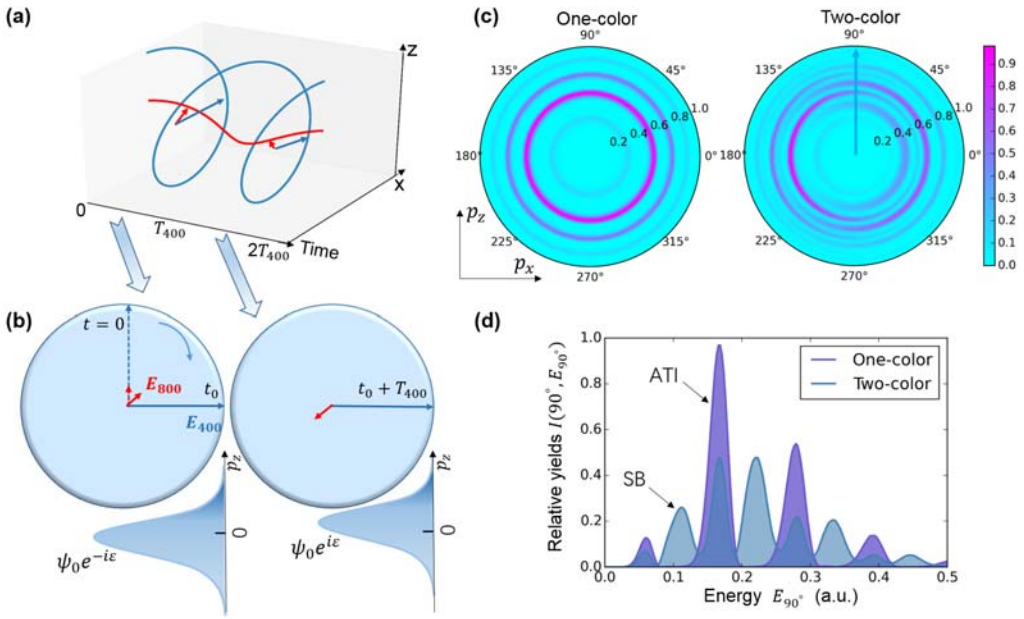

FIG. 1. Principle of double-hand attoclock photoelectron interferometer. (a) Illustration of co-rotating two-color [400 nm (ionizing) + 800 nm (weak probing)] circularly polarized laser fields at phase delay $\varphi_L = 0$. The arrows indicate their electric-field vectors (like two hands of a clock) at a pair of ionization instants, t_0 and $t_0 + T_{400}$, where T_{400} is a period of 400 nm field. (b) The track of the clock hands in the polarization plane and the laser-induced EWPs at t_0 and $t_0 + T_{400}$. At time zero the two clock hands (dashed arrows) are parallel, and then two clock hands start to rotate with different angular velocities. At the two interfering ionization instants, the directions of the ionizing field (long clock hand) are same and those of the short clock hand are opposite, leading that the potential barrier is modulated inversely. The perturbative clock hand leaves opposite effects during ionizing, and thus the EWPs record the sub-barrier information in their amplitudes and phases, which finally will be mapped into the modification of their interference pattern compared with that in absence of the probe light. (c) Photoelectron momentum distributions simulated by the SFA model. The final interference fringe between the EWPs illustrated in (b) is

marked with the arrow in direction of polar angle 90°. (d) The photoelectron energy distribution from (c) along the polar angle 90°.

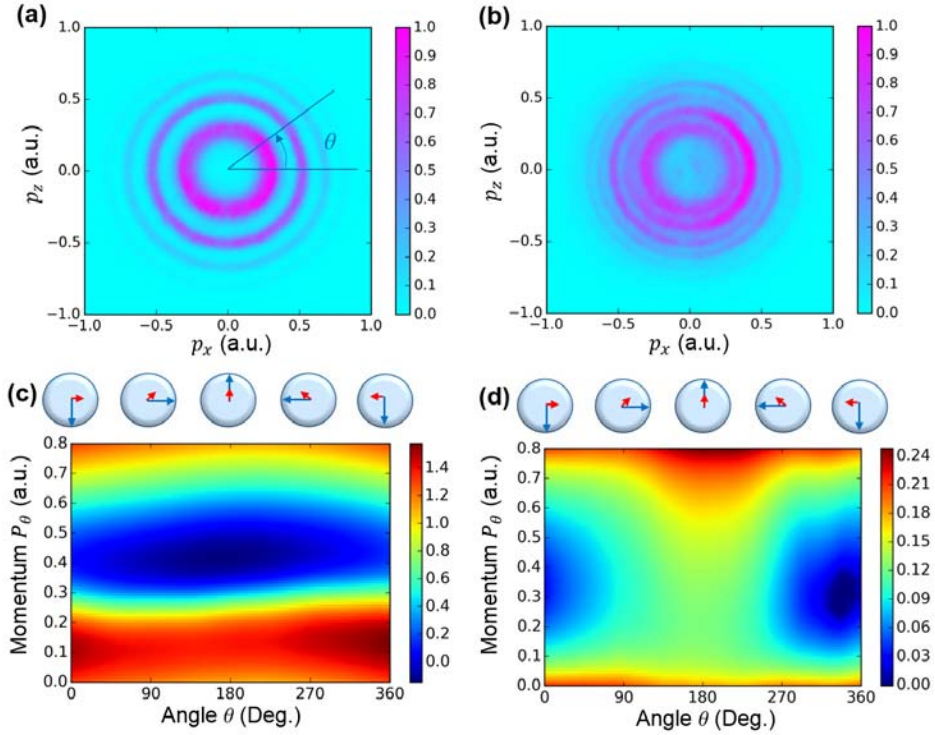

FIG. 2. Measured photoelectron momentum distributions in single (a) and co-rotating (b) circularly polarized fields at phase delay φ_L = 0. The extracted real phase $\mathrm{Re}[\varepsilon(\boldsymbol{p}_\theta,\theta)]$ (c) and imaginary phase $\mathrm{Im}[\varepsilon(\boldsymbol{p}_\theta,\theta)]$ (d) from the above measured distributions. The ionization instants are marked on the top of (c) and (d).

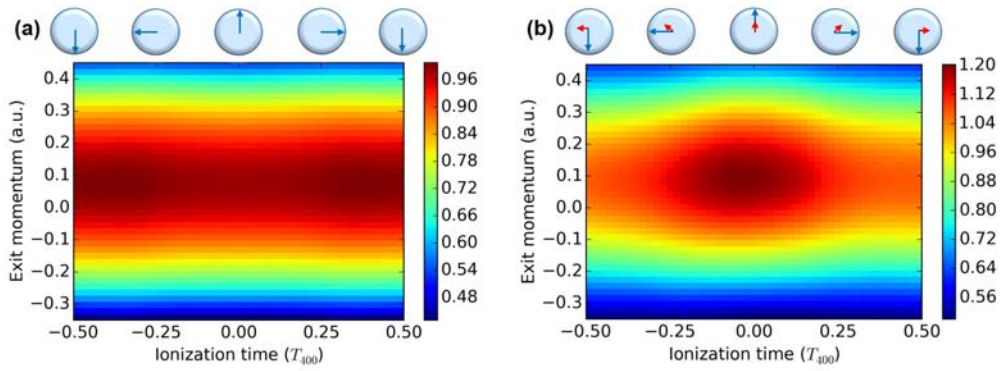

FIG. 3. Dynamic imaging of emitting EWPs. Reconstructed attosecond-resolved emitting EWPs in momentum space in one-hand attoclock (a) and double-hand attoclock (b).

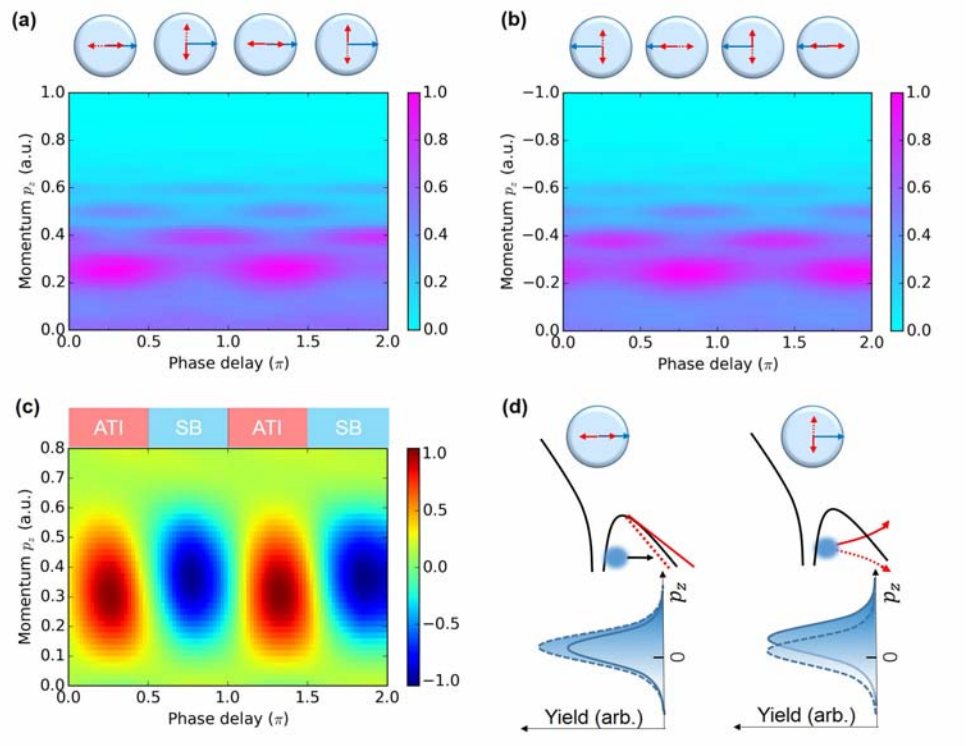

FIG. 4. Scanning short clock-hand working mode of the double-hand attoclock photoelectron interferometer. Measured electron momentum distribution along the positive p_z axis (a) and along the negative p_z axis (b) with respect to the phase delay between the two colors. p_x and p_y are both confined within a small bin [-0.02, 0.02]. The interferogram at each phase delay is contributed by two orientations of the short pointer, corresponding to the birth times of the two interfered EWPs. (c) Differential distribution between the extracted backgrounds from (a) and (b). The differential value is normalized to [-1, 1], from the SB (blue area) to the ATI (red area) dominant region. (d) The deformed Coulomb potentials and the initial momentum distributions of the EWPs when two clock hands are parallel and perpendicular, respectively. Because the long clock hand is long the x axis, the EWP approximately shows a Gaussian along p_z at the exit.